

## Limb broadening of quiet Sun transition zone lines from *OSO-8* observations

Robert Roussel-Dupré, Michael H. Francis and  
Donald E. Billings *University of Colorado, Department of Astro-Geophysics,  
Boulder, Colorado 80309, USA*

Received 1978 July 24; in original form 1978 April 20

**Summary.** From the analysis of 93 quiet Sun profiles of  $\lambda 1393$  of Si IV we conclude that line profiles from the quiet transition region do undergo a marked broadening with distance from the centre of the solar disk. Most of the broadening appears to be due to the increase of optical depth of the emitting regions towards the limb, indicating approximately isotropic disturbances. A more detailed analysis of  $\lambda 1393$  suggests that the horizontal amplitude may be somewhat greater than the radial amplitude. An analysis of the integrated intensities versus position from the centre of the disk imply  $\tau = 0.22 \pm 0.16$  for the disk centre, optical depth of Si IV  $\lambda 1393$ .

### 1 Introduction

The remarkable width of emission lines from the chromosphere–corona transition zone (approximately three times that expected from thermal broadening) has been noted by Brueckner & Kjeldseth-Moe (1971), Boland *et al.* (1973), Feldman & Behring (1974), Boland *et al.* (1975), Feldman, Doschek & Tousey (1975), Feldman *et al.* (1976) and Feldman, Doschek & Patterson (1976). The latter reported that the widths were similar at disk centre and near the limb but broadened right at the limb. Shine *et al.* (1976), using *OSO-8* data reported that the lines were broader at the limb than at the centre. The present study is a systematic analysis of quiet Sun profiles of  $\lambda 1393$  of Si IV, from accumulated *OSO-8* observations for evidence of a functional relationship between centre to limb position and width of the line. The interpretation requires a knowledge of the optical depth of  $\lambda 1393$ . We have determined the optical depth for this line by studying the integrated intensity as a function of limb position.

### 2 Data

For our study we used those quiet Sun  $\lambda 1393$  profiles in the *OSO-8* files, excluding coronal hole profiles, which had at least 75 intensity points on the profile and which had a signal/noise ratio of at least 2 at line centre.

To fit these profiles, we used a computer program developed by the *OSO-8* staff. A Gaussian profile of the form:

$$I(x) = A + B \exp[-(x - x_0)^2/\Delta^2] \quad (1)$$

is fitted to the data, where  $A$  is the background intensity,  $B$  the line centre intensity,  $x_0$  the position of line centre and  $\Delta$  the  $1/e$  half-width. The program fits a least squares Gaussian profile to the observations, by varying each parameter ( $A, B, x_0, \Delta$ ) $_n$  in turn while holding the other parameters fixed so as to minimize

$$\sum_{i=1}^n (I_i - I_{oi})^2$$

through a succession of iterations. The variance for each profile is given by

$$\frac{\sum (I_i - I_{oi})^2}{n} = \text{variance} \quad (2)$$

where  $I_i$  is the intensity given by the Gaussian function at the  $i$ th point,  $I_{oi}$  is the observed intensity at the same point, and  $n$  the number of points on the profile. In determining the average of any parameter for a number of profiles a weighting factor  $g_j = B^2/\text{variance}$  was assigned to each profile. For analysis of limb broadening we grouped out the profile according to the disk position of the observation into intervals of 0.1 in  $\mu = \cos \theta$  ( $\theta$  being the angle between the line of sight and the solar radius to the point of observation), except that near the limb the interval in  $\mu$  was decreased to 0.05, then 0.02. Averages of the line width parameter,  $\Delta$ , over each of these intervals are plotted in Fig. 1, and of the relative integrated intensity,  $B\Delta/B\Delta(\mu = 1)$ , in Fig. 2. The error bars in Fig. 1 are given by  $\sqrt{\sum g_j (\bar{\Delta} - \Delta)^2 / \sum g_j}$  and in Fig. 2 by  $\sqrt{\sum g_j (B\bar{\Delta} - B\Delta)^2 / \sum g_j}$ . These error bars appear to represent real differences among the profiles in each group, being considerably in excess of what one would expect from the variances of the observed points in the profiles from their Gaussian fit.

### 3 Theory

#### 3.1 LIMB BROADENING

We calculate here the theoretical  $1/e$  half-width,  $x$ , of a line broadened by absorption and scattering as a function of distance from the centre of the disk. For simplicity we assume

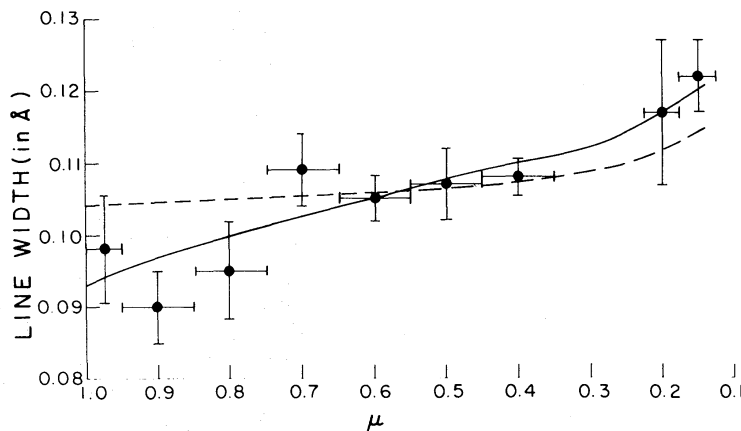


Figure 1. A plot of the  $1/e$  half-width for Si IV  $\lambda$  1393 against  $\mu$ . The dashed line represents the best isotropic fit and the solid line the best anisotropic fit.

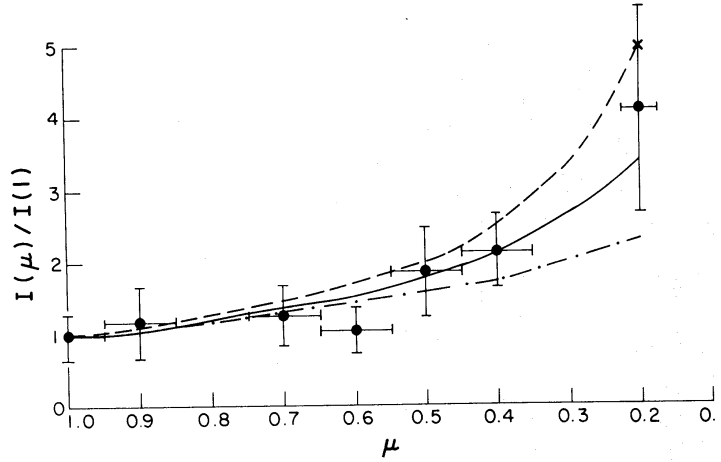


Figure 2. The ratio of the integrated intensity at  $\mu$  to that at Sun centre. Limb-brightening curves for the best fit optical depth ( $\tau = 0.22$ ) and, for comparison,  $\tau = 0.0$  and  $0.5$  are plotted.

homogeneous line-forming region of geometric thickness  $H$  and constant source function  $S$ , a reasonably good assumption over the narrow temperature range for the existence of Si IV (see Appendix).

We assume the profile function in complete redistribution to be in the form  $\exp(-x^2/\Delta_D^2)$ .  $\Delta_D$ , the  $1/e$  half-width of the profile function is a combination of both thermal and non-thermal broadening:

$$\Delta_D^2 = \Delta_T^2 + \Delta_M^2 \quad (3)$$

$$I = \int_0^\tau S \exp[-Z(p) \tau'/H] \frac{Z(p)}{H} d\tau' \quad (4)$$

where  $Z(p)$  is the thickness of the line-forming region along the line of sight,  $p = r/R$ ,  $r$  being the distance of the point of observation from the centre of the disk and  $R$  the inner radius of the emitting shell. Then for the range of  $r$  for our data:

$$(Z/H) \approx (1 - p^2)^{-1/2}. \quad (5)$$

If  $\tau_0$  is the optical depth at the centre of the line at Sun centre,  $d\tau = \exp[-(x/\Delta_D)^2]$ ,  $d\tau_0 = a d\tau_0$  and equation (4) becomes

$$I(x) = \frac{SaZ}{H} \int_0^{\tau_0} \exp[-(a\tau'_0 Z/H)] d\tau'_0 = S[1 - \exp[-(a\tau_0 Z/H)]] \quad (6)$$

At line centre,

$$I(0) = S[1 - \exp[-(\tau_0 Z/H)]] \quad (7)$$

We wish to find the value of  $x$ , such that in a redistribution broadened profile

$$\frac{I(x_1)}{I(0)} = \frac{1}{e} \quad (8)$$

Substituting (6) and (7) into (8) and solving gives

$$\left(\frac{x_1}{\Delta_D}\right) = \left\{ -\ln \frac{H}{Z\tau_0} [1 - \ln [e + e[-(\tau_0 Z/H)] - 1]] \right\}^{1/2} \quad (9)$$

$(x_1/\Delta_D)$  is the ratio of the  $1/e$  half-width of a line broadened by scattering and redistribution to the same parameter of the redistribution profile. Thus, we see that the broadening is a function of the optical depth of the centre of the line at Sun centre.

### 3.2 LIMB-BRIGHTENING AS A FUNCTION OF $\tau$ AND $\mu$ ( $= \cos \theta$ )

The ratio of integrated intensity at  $\mu$  to that at the centre of the Sun ( $\mu = 1$ ) of a line of constant source function is given by

$$\frac{I(\mu)}{I(1)} = \frac{[1 - \exp(-\tau/\mu)]}{[1 - \exp(-\tau)]} \quad (10)$$

provided  $\mu$  is not too close to 0.0. Thus, if we know the integrated intensity as a function of  $\mu$  we can determine  $\tau$ .

## 4 Results

Fig. 2 is a plot of relative integrated intensity as a function of  $\mu$ . In making a least squares fit of the form of equation (10) to determine  $\tau$ , each point was weighted by

$$\Sigma g_i \left( \frac{\overline{I(\mu)}}{I(1)} \right)^2 / \Sigma g_j \left[ \frac{\overline{I(\mu)}}{I(1)} - \left( \frac{I(\mu)}{I(1)} \right)_j \right]^2$$

where  $\Sigma_j$  is a summation over the profiles at a given  $\mu$  and  $\overline{I(\mu)}/I(1)$  is the value of the average integrated intensity ratio at  $\mu$ . We find a value for  $\tau$  of  $\tau = 0.22 \pm 0.16$ . This compares to a value of 0.24 found by Withbroe (1970). An alternative method for determining  $\tau$  is to find the ratio of the two Si IV lines  $\lambda 1393$ ,  $\lambda 1402$ . However, there was an insufficient amount of *OSO-8* data for  $\lambda 1402$  to determine this ratio.

Having determined  $\tau$  we proceeded to determine  $\Delta_M$ .  $\tau$  is the integrated optical depth over the entire line. Hence the line centre optical depth  $\tau_0$  is given by  $\tau/\sqrt{\pi}$ . We can substitute this into equation (9) to determine the ratio of line widths for the redistribution broadened line to that of the unbroadened line. To determine the line width  $\Delta_D$  of the observed profiles after redistribution broadening is removed we divide the observed points in Fig. 2 by the ratio as determined by equation (9). Then we solve for  $\Delta_M$ , using equation (3). This gives the plotted points for Fig. 3.

We now designate velocity components  $V_a$  and  $V_r$  in a plane containing the line of sight to an observed point on the Sun and the centre of the Sun.  $V_a$  is parallel and  $V_r$  is perpendicular to the Sun's surface. The third component of velocity, being perpendicular to the line of sight, does not contribute to line broadening. The line of sight components of  $V_a$  and  $V_r$

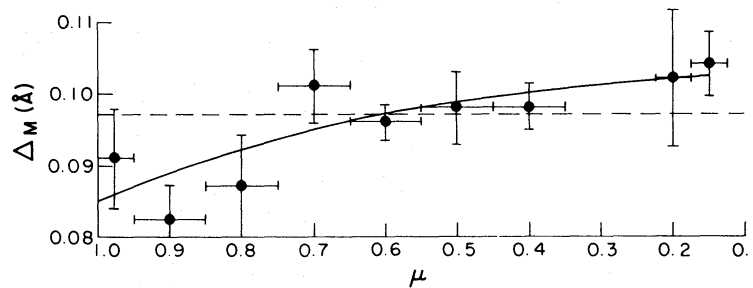


Figure 3. A plot of  $\Delta_M$  versus  $\mu$ . The dashed line is the best isotropic fit and the solid line the best anisotropic fit.

are  $V_a \sin \theta$  and  $V_r \cos \theta$ . We use a weighted least squares fit to the points in Fig. 3 to determine  $V_a$  and  $V_r$  according to:

$$\Delta_M^2 = V_a^2 \sin^2 \theta + V_r^2 \cos^2 \theta \quad (11)$$

where the weighting is analogous to that used for fitting the points of Fig. 2.

$V_a$  and  $V_r$  so determined are the velocity components at the 1/e points of their Gaussian distributions. They are

$$V_a = 19.54 \pm 2.59 \text{ km/s,}$$

$$V_r = 17.09 \pm 3.79 \text{ km/s.}$$

Dividing each by  $\sqrt{2}$  gives the corresponding rms velocities:

$$\sqrt{V_a^2} = 12.08 \pm 2.68 \text{ km/s,}$$

$$\sqrt{V_r^2} = 13.81 \pm 1.83 \text{ km/s.}$$

Thus,  $V_a/V_r = 1.14 \pm 0.28$ .

If we assume the microturbulence to be isotropic, we find, for each component of velocity,

$$V = 18.50 \pm 2.94 \text{ km/s,}$$

$$\sqrt{V^2} = 13.08 \pm 2.08 \text{ km/s.}$$

Now that we have the theoretical  $\Delta_m(\mu)$  we can find the theoretical  $\Delta_D(\mu)$ . We can then put  $\Delta_D(\mu)$  into equation (9) to find a theoretical curve for  $x_1(\mu)$ . It is these curves that are plotted in Fig. 1. One is for isotropic microturbulence and one is for the anisotropic fit.

## 5 Discussion

The suggestion of greater horizontal than vertical velocities (or even isotropic velocities) anywhere above the chromosphere is a marked departure from the Schwarzschild (1948) picture of upward moving acoustic waves heating the corona. There are many processes which might generate horizontally directed velocities: refracted or reflected acoustic waves, upward moving Alfvén waves and fast mode MHD waves. In our data the anisotropic effect is not strong and has a certainty level of only about 60 per cent.

We attempted to make the same analysis for CIV  $\lambda 1548$ . However, even though the profiles appeared to be of about the same quality as for  $\lambda 1393$ , there was a great deal more scattering both in the limb-brightening and limb-broadening data. This suggests that inhomogeneities may play a much more important role in the CIV  $\lambda 1548$  than in Si IV  $\lambda 1393$  emission, even though these lines are formed only 20 000 K apart (Summers 1974).

## Acknowledgments

This research was supported by the National Science Foundation Grant No. ATM 76-04048. The authors wish to thank the personnel of the OSO-8 project for the opportunity to participate as guest investigators.

## References

- Boland, B. C., Dyer, E. P., Firth, J. G., Gabriel, A. H., Jones, B. B., Jordan, C., McWhirter, R. W. P., Monk, P. & Turner, R. F., 1975. *Mon. Not. R. astr. Soc.*, 171, 697.  
 Boland, B. C., Engstrom, S. F. T., Jones, B. B. & Wilson, R., 1973. *Astr. Astrophys.*, 22, 161.

- Brueckner, G. E. & Kjeldseth-Moe, O., 1971. *Space Res.*, **12**, 1595.  
 Doschek, G. A., Feldman, U. & Tousey, R., 1975. *Astrophys. J.*, **202**, L151.  
 Feldman, U. & Behring, W. E., 1974. *Astrophys. J.*, **189**, L45.  
 Feldman, U., Doschek, G. A. & Patterson, N. P., 1976. *Astrophys. J.*, **209**, 270.  
 Feldman, U., Doschek, G. A. & Tousey, R., 1975. *Astrophys. J.*, **202**, L147.  
 Feldman, U., Doschek, G. A., Van Hoosier, M. E. & Purcell, J. D., 1976. *Astrophys. J. Suppl.*, **31**, 445.  
 Schwarzschild, M., 1948. *Astrophys. J.*, **107**, 1.  
 Shine, R. A., Roussel-Dupré, D., Bruner, E. C., Jr, Chipman, E. G., Lites, B. W., Rottman, G. J., Athay R. G. & White, O. R., 1976. *Astrophys. J.*, **210**, L107.  
 Summers, H. P., 1974. *Mon. Not. R. astr. Soc.*, **169**, 663.  
 Withbroe, G. O., 1970. *Sol. Phys.*, **11**, 208.

### Appendix: justification of constant source function

Since the source function includes resonance scattering:

$$S_\nu = (1 - \epsilon)\bar{J} + \epsilon B_\nu \approx \bar{J} + \epsilon B_\nu \quad (\text{A1})$$

where, for complete redistribution

$$\bar{J} = \int_{-\infty}^{\infty} \phi_\nu J_\nu d\nu,$$

$\phi_\nu$  is the absorption profile and  $\epsilon = (C_{21}/A_{21}) \sim 10^{-4}$  for Si IV.

Under complete redistribution the emission and absorption profiles are the same and thus,

$$\epsilon B_\nu = \frac{C_{21}}{A_{21}} [1 - \exp(-h\nu_0/kT)] \quad (\text{A2})$$

and is independent of  $\nu$ .

$J_\nu$  is given by

$$J_\nu = \frac{1}{2} \int_{-1}^1 \int_0^{\tau_\nu} S(t) \exp(-t_\nu/\mu) \frac{dt_\nu}{\mu} d\mu. \quad (\text{A3})$$

Thus,  $\bar{J}$  is

$$\bar{J} = \frac{1}{2} \int_{-\infty}^{\infty} \int_{-1}^1 \int_0^{\tau_\nu} S(t) \exp(-t_\nu/\mu) \frac{dt_\nu}{\mu} d\mu d\nu \phi_\nu. \quad (\text{A4})$$

If we now assume  $S(t)$  is independent of optical depth and  $\tau_\nu = \tau\phi_\nu$  and integrate over  $t$  we find

$$\bar{J} = \frac{S}{2} \int_{-\infty}^{\infty} \int_{-1}^1 [1 - \exp(-\phi_\nu\tau/\mu)] d\mu \phi_\nu d\nu. \quad (\text{A5})$$

Integrating over  $\mu$  we obtain

$$\bar{J} = S \int_{-\infty}^{\infty} [\phi_\nu - \phi_\nu E_2(\tau\phi_\nu)] d\nu \quad (\text{A6})$$

or

$$\bar{J} = S \left[ 1 - \int_{-\infty}^{\infty} \phi_{\nu} E_2(\tau \phi_{\nu}) \right] d\nu. \quad (\text{A7})$$

$$E_2(\phi_{\nu} \tau) \sim [1 - \tau \phi_{\nu} + \tau \phi_{\nu} (\gamma + \ln \tau \phi_{\nu})] \quad (\text{A8})$$

for  $\tau \phi_{\nu} \ll 1$ , where  $\gamma = 0.5772$ .

Now, on the assumption that  $S$  was constant we found  $\tau = 0.22 \pm 0.16$  or  $\tau < 0.38$  hence,  $\tau \phi_{\nu} < 0.22$ , which justifies the approximation in (A8).

Substituting (A8) into (A7) and integrating we find

$$\bar{J} = 0.47 S \tau. \quad (\text{A9})$$

Now  $S = \bar{J} + \epsilon B$  and if we substitute this into (A9) we find

$$\bar{J} = 0.47 \epsilon B \tau.$$

We can substitute this back into (A4) and iterate and if we continue to do this we get the series

$$\bar{J} = 0.47 \tau (1 + 0.47 \tau - (0.47 \tau)^2 + (0.47 \tau)^3 - \dots) \epsilon B. \quad (\text{A10})$$

Thus  $S$  is given by

$$S = \epsilon B [1 + 0.47 \tau (1 + 0.47 \tau - (0.47 \tau)^2 + (0.47 \tau)^3 - \dots)]. \quad (\text{A11})$$

Hence, even if  $\tau = 0.38$ ,  $S$  is constant to 20 per cent.